

Theory, Experiment and Computer Simulation of the Electrostatic Potential at Crystal/Electrolyte Interfaces

Piotr Zarzycki,^{a,*} Kevin M. Rosso,^a Shawn Chatman,^a
 Tajana Preočanin,^b Nikola Kallay,^b and Wojciech Piasecki^c

^aChemical and Materials Sciences Division, Pacific Northwest National Laboratory, Richland, WA 99354, USA

^bLaboratory of Physical Chemistry, Department of Chemistry, Faculty of Science, University of Zagreb, HR 10000 Zagreb, Croatia

^cDepartment of Biochemistry, The Jozef Pilsudski Academy of Physical Education, Warsaw, Poland

RECEIVED JUNE 16, 2010; REVISED OCTOBER 1, 2010; ACCEPTED OCTOBER 5, 2010

Abstract. In this feature article we discuss recent advances and challenges in measuring, analyzing and interpreting the electrostatic potential development at crystal/electrolyte interfaces. We highlight progress toward fundamental understanding of historically difficult aspects, including point of zero potential estimation for single faces of single crystals, the non-equilibrium pH titration hysteresis loop, and the origin of nonlinearities in the titration response. It has been already reported that the electrostatic potential is strongly affected by many second order type phenomena such as: surface heterogeneity, (sub)surface transformations, charge transfer reactions, and additional potential jumps at crystal face edges and/or Schottky barriers. Single-crystal electrode potentials seem particularly sensitive to these phenomena, which makes interpretation of experimental observations complicated. We hope that recent theory developments in our research group including an analytical model of titration hysteresis, a perturbative surface potential expansion, and a new surface complexation model that incorporates charge transfer processes will help experimental data analysis, and provide unique insights into the electrostatic response of nonpolarizable single-crystal electrodes.

Keywords: single-crystal electrode, surface potential, Nernst potential, computer simulations, electron transfer, metal oxide

INTRODUCTION

Metal (hydr)oxides acquire a surface electric charge when brought into contact with an aqueous solution.^{1,2} Molecular and/or dissociative adsorption of water molecules is a probable mechanism of obtaining surface charge at metal-terminated surface sites, whereas proton uptake is a more probable scenario for oxygen-terminated surface sites.³ Because actual metal oxide surfaces are typically structurally nonuniform, both charging mechanisms play an important role. Surface sites exhibit an amphoteric property, that is they are able to uptake or release protons and thus form negatively, neutral, or positively charged surface groups.^{1,2} The net balance of protons at the metal oxide/aqueous interface is a primary charging mechanism, and for this reason H⁺ and OH⁻ ions play a key role as potential determining ions (PDI). Electrolyte ion association with surface sites is considered a secondary process, which results in formation of inner- or outer-sphere surface complexes.¹

These phenomena that govern the development of the electrical interfacial layer are thought to be general across a wide range of metal (hydr)oxides, including more broadly oxides of metalloids such as silicon.⁴ Representative microscopic and macroscopic models of electrical interfacial layers formed at metal oxide/electrolyte interfaces are shown in Figure 1, and include those that can be constructed using molecular simulation (Figure 1a), surface complexation modeling (Figure 1b), and analytical macroscopic theories (Figure 1c).

Experimental characterization of metal (hydr)oxide acid-base properties involves determination of the surface charge (σ_0), surface potential (ψ_0), or ζ -potential as a function of pH. Surface charge is the most frequently reported characteristic, and it is typically obtained from potentiometric titration of a microparticulate metal oxide suspension.^{1,5,6} The electrokinetic potential (ζ) is usually obtained in an electrophoretic experiment.⁷ The surface potential is the most difficult property to determine experimentally. The difficulties lie in both the

* Author to whom correspondence should be addressed. (E-mail: Piotr.Zarzycki@pnl.gov or zarzycki.piotrek@gmail.com)

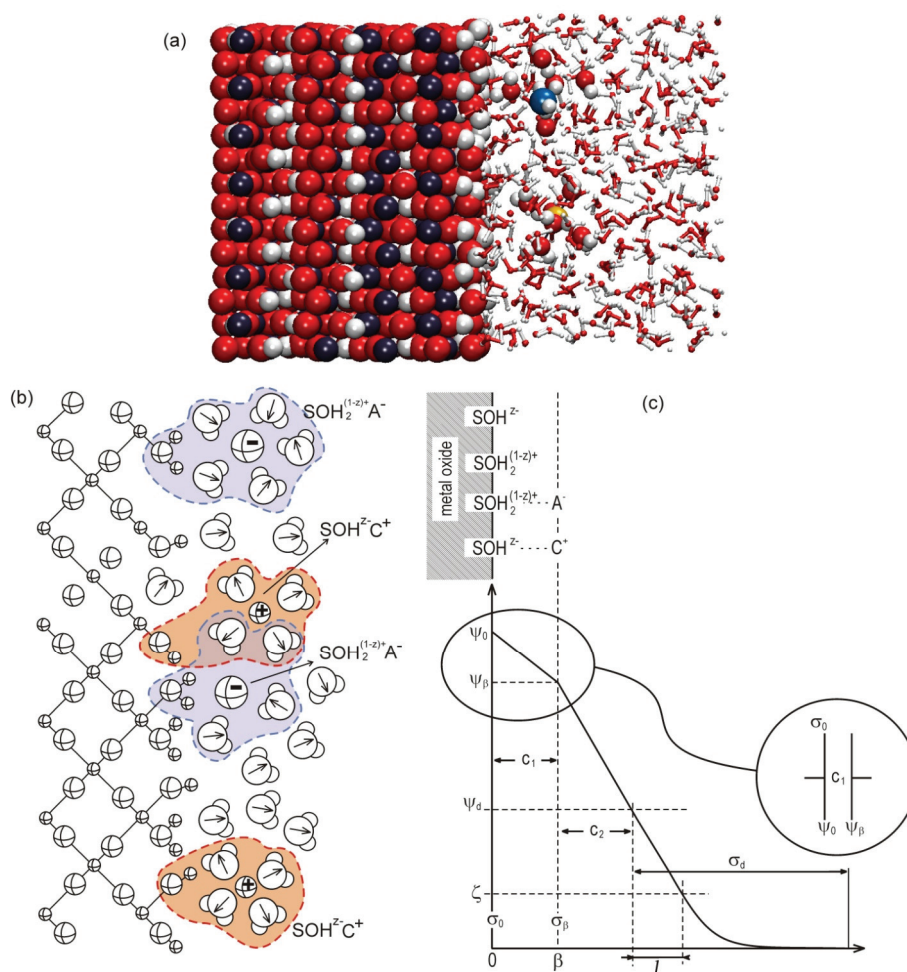


Figure 1. (a) Molecular representation of the electrical interfacial layer at the goethite (101)/electrolyte interface (using a snapshot of the computation cell used in the molecular dynamics simulations of the goethite/electrolyte interface from Reference 86); (b) the metal oxide/electrolyte interface with inner- and outer-sphere surface complexes (e.g., of surface associated electrolyte ions); (c) simplified double-layer picture of an electrical interfacial layer at the metal oxide/electrolyte interface provided by the Surface Complexation Model. The surface, β -plane and diffuse potentials (ψ_0 , ψ_β , ψ_d) are correlated through the capacity constants (c_1 , c_2). The ζ -potential is the potential at the slip plane located at the distance l from the beginning of a diffuse layer.

construction of a sensor electrode and in finding a relationship between measured cell voltage and the surface potential.

After introducing the methods and tools used for studying the surface potential at single crystal electrodes, we briefly discuss recent associated challenges along with some proposed solutions, which were developed in a combined two-team effort: Kevin M. Rosso's research group at the Pacific Northwest National Laboratory, Washington, U.S.A., and Nikola Kallay's research group at the University of Zagreb in Croatia.

Electrical Interfacial Layer Near the Nonpolarizable Electrode

Metal (hydr)oxide electrodes are an example of nonpolarizable (depolarized) electrodes, whose response does

not depend on the externally applied potential. However, electrical interfacial layer formation causes a flow of charging current through the cell.⁸ This current is an example of non-Faradaic current (i.e., not related to reduction-oxidation processes)⁸ and it decays as the interfacial charge distribution approaches the equilibrium condition of zero net current. When the potential is measured between the metal oxide electrode and a standard reference electrode (usually an ideal nonpolarizable electrode), then we observe a voltage drop representing the charging current, which is described by Ohm's law:⁸

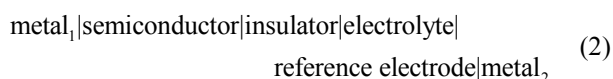
$$V = iR \quad (1)$$

where i is the charging current passing through the cell and R describes the collective resistance of the setup and instrument. The absolute electrode potential is un-

available, only the potential difference between the metal oxide electrode and reference electrode can be directly measured.^{8,9} This voltage measurement, sometimes referred to as an open circuit potential or rest potential measurement, can be conducted in either a two or three electrode configuration. The two-electrode setup is justified when the current that is passed through the circuit is small, such as the case with a high instrument resistance (or impedance) and/or low measured potentials ($V < 1\text{--}2$ mV).⁸ In the case of larger currents the voltage measurements should be conducted using a three-electrode setup, in which an auxiliary electrode (counter electrode) is used as the current sink for the cell, and to ensure that the potential difference is measured as close as possible to the zero net current (equilibrium) condition. It is worth mentioning that the auxiliary electrode cannot completely eliminate the potential drop due to electric interfacial layer equilibration. There is still a fraction of solution resistance which remains uncompensated.⁸ The resistance of nonpolarizable-electrode/electrolyte interfaces also strongly depends on how the working electrode is constructed. For determination of metal oxide surface potentials, three kinds of working electrodes have been used so far: (i) one based on the ion sensitive field-effect transistor (ISFET),^{10–12} (ii) one using a metallic wire covered by the metal oxide in a fine particulate form^{13–16} and (iii) one using a single-crystal electrode, typically in which a single face of the crystal is exposed to solution (SCrE).^{17–21}

Ion-Sensitive Field Effect Transistor Electrode

An electrode based on the ISFET consists of a metal attached to a semiconductor (*e.g.*, Si) whose surface is covered by the phase of interest, an insulator (*e.g.*, SiO₂) which is in contact with an electrolyte.^{10,11} A typical electrochemical cell with an ISFET electrode has the following construction:^{10,11}



An experimental observable in this configuration is the flat-band potential of the semiconductor, that is, the voltage applied to the metal (metal₁) which makes the semiconductor surface potential zero (the zero band bending condition).^{10,11} The measured flat-band voltage of the semiconductor is particularly sensitive to the potential drop at the insulator/electrolyte interface which, in turn, is developed due to metal oxide surface protonation. This is the reason that the ISFET electrode can be useful as a chemically sensitive electronic device for H⁺ ion detection.^{10,11} Although ISFET electrodes are rarely used to determine the surface potential of metal

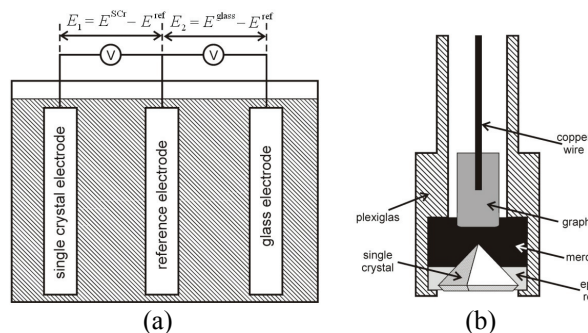


Figure 2. (a) one possible design of an open circuit potential setup for surface potential measurements using a single-crystal electrode; (b) a possible method for constructing the single-crystal electrode.

oxides, the first analytical models of ψ_0 were built based on ISFET electrode measurements.

Coated Wire Electrodes

The surface potential of the metal oxide/electrolyte interface can also be examined by using a coated wire electrode, that is, a metallic wire covered by the metal oxide.^{13–16} Measurements using Pt/hematite ($\alpha\text{-Fe}_2\text{O}_3$),¹³ Ti/TiO₂¹⁴ or Pd/PdO^{15,16} electrodes serve as a good illustration of this method. Due to the intrinsic porosity of the metal oxide layer in this approach, electrolyte ions are in simultaneous contact with both the metal oxide and the metallic core. Redox reactions occurring at the metallic core therefore contribute substantially to the measured potential, consequently the electrode behaves as a so-called electrode of the second-kind.²² Despite this aspect, if the contribution from the metallic core is sufficiently well understood or predictable, this configuration does provide useful information about the metal oxide surface potential. However, such problems arising from metal oxide porosity are completely eliminated by the single-crystal electrode method.

Single-crystal Electrode

The concept of using a single-crystal as an electrode goes back many years (*e.g.*, Quinn *et al.*²³). However, this approach has recently begun to be used again as a means to access detailed information about the behavior at individual crystallographic terminations for face-specific electrical interfacial layer properties. Detailed studies have been introduced for ice crystals,^{24,25} and then adapted to single-crystals of hematite.^{17,18} The basic idea is to selectively expose only a single crystal face and measure the potential developed at its interface with electrolyte, an experiment typically performed using the three-electrode setup. The cell and one method for constructing such an electrode are schematically presented in Figure 2. In order to assure electrochemical

equilibrium, the cell potential is measured in the open circuit fashion. The current through the circuit should be kept small, requiring that the resistance of the potentiometer setup is several orders of magnitude higher than that of the single-crystal electrode. The surface potential is measured as the difference between reference and SCrE electrodes. Simultaneously, the pH is recorded using a glass electrode with respect to the same reference electrode. More detailed discussion on construction and preparation of a single-crystal electrode (SCrE) can be found in papers by Kallay and coworkers.^{17–21,26,27}

The electromotive force of the cell is simply the potential difference between the single-crystal electrode (the working electrode) and the reference electrode, that is:²⁸

$$E = E^{\text{SCrE}} - E^{\text{ref}} \quad (3)$$

which can be expressed as the inner potential differences at both interfaces (Galvani potentials)^{9,28} (considering only monovalent ions):

$$E = \Delta \phi^{\text{SCrE/sol}} - \Delta \phi^{\text{ref/sol}} - \frac{1}{F} \sum (\mu_i^{\text{SCrE/sol}} - \mu_i^{\text{ref/sol}}) - C \quad (4)$$

where $\Delta \phi^{\text{x/sol}}$ expresses the Galvani potential at the given electrode (x)/electrolyte interface, the last term expresses the difference in chemical potential of charge carriers near the SCrE and reference electrodes, and C is a constant representing all remaining potential jumps in the circuit unrelated to the surface reactions (presumably independent of PDI concentration). The Galvani potential is a difference in the electrostatic potential felt by a given ion in the interior of both phases, which is exactly the electric work required to transfer this ion from the interior of one phase to the interior of the other.^{9,28} The potential arising from the reference electrode is by definition only a voltage shift with respect to the standard hydrogen electrode, and it can be put into the constant C , giving finally the expression: $E = \Delta \phi^{\text{SCrE/sol}} - C$. In addition, simultaneous measurement of the potential difference between the auxiliary and reference electrodes allows one to monitor the variation in the bulk electrolyte pH.

The surface charge changes due to net proton release or uptake, and it usually does not involve the diffusion of H^+ ions inside the solid metal oxide phase. For this reason, the electrostatic work of transferring protons adsorbed at the metal oxide surface into the interior of metal oxide (surface potentials, χ^{SCrE}) can be neglected in the Galvani potential. In other words, the Galvani potential ($\Delta \phi^{\text{x/sol}}$) in Equation (4) can be replaced by the by Volta potential ($\Delta \psi^{\text{x/sol}}$). However, some part of the surface contribution arising from reorientation of water molecules in the strong electrostatic field generat-

ed by surface charges and adsorbed counter ions is still present. In analytical modeling, this remaining surface potential contribution is assumed to be constant during variation in surface charge (and potential).²⁹ In addition, it is expected that only the single-crystal electrode is sensitive to the change in the bulk pH; all other terms are considered as a constant shift of ψ_0 (denoted by E_T):^{26,27}

$$\psi_0 = E - E_T = \Delta \phi^{\text{SCrE/sol}} - C - E_T \quad (5)$$

Moreover, the surface potential is related to the change in the free energy of surface protonation. For instance, by assuming a single protonation step we can write:

$$\Delta G = -eN\psi_0 \quad \text{where } \Delta G = \Delta G^\circ + Nk_B T \ln Q, \quad (6)$$

and in equilibrium $\Delta G^\circ = -Nk_B T \ln K_+$

where e is the elementary charge, N is the Avogadro constant ($F = eN$ is the Faraday constant), k_B is the Boltzmann constant ($R = Nk_B$ is the gas constant), Q is the reaction quotient for protonation reaction, which in equilibrium ($\Delta G = 0$) is equivalent to the equilibrium constant (K_+). From Equation 6 we can obtain the Nernst equation:

$$\psi_0 = \frac{k_B T}{e} \ln K_+ - \frac{k_B T}{e} \ln [\text{H}^+] = \frac{2.303 k_B T}{e} (\text{PZC} - \text{pH}) \quad (7)$$

where $\text{pH} = -\log[\text{H}^+]$ and PZC is a point of zero charge defined by the intrinsic protonation constant (K_+ or a combination of equilibrium constants if more than one protonation reaction is postulated, see Analytical Models section). The Nernst equation (Equation 7) can be also derived by assuming equality of electrochemical potentials of H^+ ions at the surface and in the bulk (the equilibrium condition).²⁹

At $\text{pH} = \text{PZC}$, the surface charge and potential are zero. This requirement is used in the experimental procedure to transform the measured cell potential to the surface potential (by choosing that E_T is equal to the measured cell voltage at $\text{pH} = \text{PZC}$). More detailed discussion on transforming $E = f(\text{pH})$ into $\psi_0 = f(\text{pH})$ can be found below in the Challenges section.

To this point we have briefly introduced the fundamentals of surface measurement using the metal oxide/electrolyte interface as an example. Extension of these concepts to the other nonpolarizable surfaces, in particular to the silver halides as a key model system for example, is straightforward, requiring replacement of H^+ ion concentration (the principal PDI for metal oxide) by the silver or halide ion concentration. Silver halide is a well studied model nonpolarizable electrode material with a relatively simple composition and structure (rocksalt).^{26,29,30} At the interface between a silver halide surface and electrolyte, the source of surface charge

development is thought to be a combination of an uneven adsorption of charged ions and incongruent surface dissolution. In this case, ions common to the electrode composition (Ag^+ or halide anions) play the role of PDIs. For a long time it has been generally believed that silver halides are the Nernstian electrodes, that is, the slope of ψ_0 is approximately -59 mV/pPDI unit at room temperature (pPDI = $-\log[\text{PDI}]$).³⁰ However, Kallay, Preočanin and Šupljika^{26,27} have recently reported that the actual potential measured at the single crystal AgBr and AgI electrodes has a slightly lower slope than the Nernstian one (by about 12 %).

Analytical Models of Surface Potential

One of the first analytical expressions for the surface potential at nonpolarizable electrodes such as metal oxides was derived by Bousse *et al.*,^{10,11} and it is based on measurements using ISFET electrodes. By considering only the primary source of surface charge, namely surface protonation, Bousse *et al.*^{10,11} arrived at the following expression for surface potential as a function of pH:

$$2.303(\text{PZC} - \text{pH}) = \frac{e\psi_0}{k_{\text{B}}T} + \arcsin\left(\frac{e\psi_0}{\beta k_{\text{B}}T}\right) \quad (8)$$

where β is a system-dependent parameter which describes the deviation of ψ_0 from Nernstian behavior. The function arcsin can be replaced by its power expansion:³⁰

$$2.303(\text{PZC} - \text{pH}) = \frac{e\psi_0}{k_{\text{B}}T} + \sum_{j=0}^{\infty} \frac{(-1)^j (2j)!}{2^{2j} (j!)^2 (2j+1)} \left(\frac{e\psi_0}{\beta k_{\text{B}}T}\right)^{2j+1} \quad (9)$$

and for small values of ψ_0 , we can neglect all terms except $j = 0$, which leads to the so-called quasi-Nernstian formula:^{10,30}

$$\psi_0 = \left(\frac{\beta}{\beta+1}\right) \frac{2.303k_{\text{B}}T}{e} (\text{PZC} - \text{pH}) = \alpha \frac{2.303k_{\text{B}}T}{e} (\text{PZC} - \text{pH}) \quad (10)$$

The prefactor $\beta/(\beta+1)$ is usually expressed as a single parameter (α), which describes the decrease in the electrode response with respect to the ideal Nernstian behavior. Values for this parameter are typically obtained by indirect fitting of a surface complexation model entailing a presumed function for the relationship $\psi_0 = f(\text{pH})$. For instance, α has been found to be about 0.8 for alumina, 0.9 for TiO_2 , 0.75 for SiO_2 and approximately

0.95 for Ta_2O_5 /electrolyte interfaces (see Reference 31 and references therein).

In the case of direct experimental ψ_0 -measurement, deviation from Nernstian behavior (parameter α) is estimated by linear regression of experimental data or if possible by the following numerical derivative:³⁰

$$\alpha = -\frac{e}{2.303k_{\text{B}}T} \frac{d\psi_0}{d\text{pH}} \quad (11)$$

From here one can see that α is directly related to the variation in protonation free energy due to changes in the bulk pH by combining Equations (6) and (11) to obtain:

$$\alpha = \frac{1}{2.303k_{\text{B}}T} \frac{d\Delta G}{d\text{pH}} \quad (12)$$

For simplicity of notation, we assume that the point of zero potential is independent of electrolyte concentration, that is, that the PZC referred to here is also the point of zero salt effect.³² This is equivalent to making the assumption that there is no preferential specific ion adsorption (*i.e.*, both electrolyte ions have similar surface affinity constants). In this idealized case, the point of zero charge (the pH at which $\sigma_0 = 0$) is equal to the point of zero potential (the pH at which $\psi_0 = 0$) and to the isoelectric point (the pH at which $\zeta = 0$). In the more complex case of preferential adsorption of one electrolyte ion relative to another, these equalities can diverge and additional nomenclature has to be introduced (see papers by Kallay and coworkers for details^{17-21,26}). Effects arising from preferential specific ion adsorption are discussed in the Challenges section.

Surface Potential in Surface Complexation Models

The surface potential can be also expressed in the framework of surface complexation modeling, that is, as a function of the surface concentrations of protonated and deprotonated metal oxide surface groups. In the case of the so-called 1-pK model,³³ the surface proton balance is described by a single reaction:



with an intrinsic equilibrium constant defined as:

$$K_+ = \frac{\{\text{SOH}_2^{+1/2}\}}{\{\text{SOH}^{-1/2}\}[\text{H}^+]^{\text{int}}} \quad (14)$$

where $\{\}$ brackets stand for the equilibrium surface concentration of protonated, deprotonated sites, whereas

$[]^{\text{int}}$ stands for the concentration of the unbound surface protons. The concentration of H^+ ions at the surface can be connected to the bulk H^+ ion concentration by using the Boltzmann distribution:

$$[\text{H}^+]^{\text{int}} = [\text{H}^+]^{\text{bulk}} \exp\left(-\frac{e\psi_0}{k_B T}\right) \quad (15)$$

By inserting Equation (15) into Equation (14) we can define the surface potential as follows:^{17-19,34}

$$\begin{aligned} \psi_0 &= \frac{2.303k_B T}{e}(\text{PZC} - \text{pH}) - \frac{k_B T}{e} \ln \frac{\{\text{SOH}_2^{+1/2}\}}{\{\text{SOH}^{-1/2}\}} \\ &= \frac{2.303k_B T}{e}(\text{PZC} - \text{pH}) - \frac{k_B T}{e} \ln \frac{\theta_+}{\theta_-} \end{aligned} \quad (16)$$

where $\text{PZC} = -\text{p}K_+$, and θ_+, θ_- stand for the fractional occupation for positively and negatively charged surface groups at a given pH (*i.e.*, from use of an adsorption isotherm curve ($\theta_i = [i]/N_s$, where is the surface site density). Equation (16) predicts deviation from the Nernst equation as a function of surface protonation/deprotonation processes; accordingly the previously introduced parameter α can be redefined as:³⁰

$$\alpha = 1 - \frac{1}{2.303(\text{PZC} - \text{pH})} \ln \frac{\theta_+}{\theta_-} \quad (17)$$

which is well defined only for $\text{pH} \neq \text{PZC}$ and $\theta_i \neq 0$ (but can be estimated in the limit $\text{PZC} - \text{pH} \rightarrow 0$ by employing the Bernoulli-l'Hospital rule, see Reference 30). In the case of linear surface potential $\alpha = \text{const.}$ and consequently $(\ln(\theta_+/\theta_-))/(\text{PZC} - \text{pH}) = \text{const.}$, otherwise α becomes a function of pH.

In the case of the 2-pK model,^{35,36} proton uptake/release is described by two surface reactions:



with equilibrium constants defined as:

$$K_1 = \frac{\{\text{SOH}\}}{\{\text{SO}^-\}[\text{H}^+]^{\text{int}}} \quad \text{and} \quad K_2 = \frac{\{\text{SOH}_2^+\}}{\{\text{SOH}\}[\text{H}^+]^{\text{int}}} \quad (19)$$

By replacing surface H^+ concentration by the bulk one (Equation 15), and rewriting both equations in order to eliminate $[\text{SOH}]$, we can define the surface potential as:¹⁷⁻¹⁹

$$\begin{aligned} \psi_0 &= \frac{2.303k_B T}{e}(\text{PZC} - \text{pH}) - \frac{k_B T}{2e} \ln \frac{\{\text{SOH}_2^{+1/2}\}}{\{\text{SOH}^{-1/2}\}} \\ &= \frac{2.303k_B T}{e}(\text{PZC} - \text{pH}) - \frac{k_B T}{2e} \ln \frac{\theta_+}{\theta_-} \end{aligned} \quad (20)$$

where $\text{PZC} = -(\text{p}K_1 + \text{p}K_2)/2$. Again, we can try to express the parameter α from Equation (10) as a function of surface coverage:

$$\alpha = 1 - \frac{1}{4.606(\text{PZC} - \text{pH})} \ln \frac{\theta_+}{\theta_-} \quad (21)$$

Finally, in the case of the multisite complexation model (MUSIC),^{37,38} wherein surface sites are treated as possessing fractional charge whose magnitude (z) depends on the effective metal ion coordination, the general protonation reaction can be written as follows (using a single protonation reaction as an analogue of the 1-pK model):³⁴



with the equilibrium constant defined as:

$$K = \frac{\{\text{SOH}_2^{1-z}\}}{\{\text{SOH}^{z-}\}[\text{H}^+]^{\text{int}}} \quad (23)$$

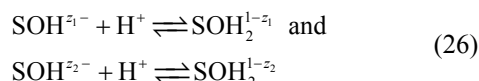
Applying a similar procedure of replacing surface H^+ concentration by the bulk one (Equation (15)) allows us to express the surface potential as:³⁴

$$\begin{aligned} \psi_0 &= \frac{2.303k_B T}{e}(\text{PZC} - \text{pH}) - \frac{k_B T}{e} \ln \frac{(1-z)\{\text{SOH}_2^{1-z}\}}{z\{\text{SOH}^{z-}\}} \\ &= \frac{2.303k_B T}{e}(\text{PZC} - \text{pH}) - \frac{k_B T}{e} \ln \frac{\theta_+}{\theta_-} \end{aligned} \quad (24)$$

Now the deviation from the Nernst response (α) can be expressed as:

$$\alpha = 1 - \frac{1}{2.303(\text{PZC} - \text{pH})} \ln \left[\frac{1-z}{z} \frac{\theta_+}{\theta_-} \right] \quad (25)$$

In the two-reaction version of the MUSIC model,^{37,38} surface protonation is described as:



and the corresponding intrinsic equilibrium constants are given by:

$$K_1 = \frac{\{\text{SOH}_2^{1-z_1}\}}{\{\text{SO}^{(z_1+1)-}\}[\text{H}^+]^{\text{int}}} \text{ and } K_2 = \frac{\{\text{SOH}_2^{1-z_2}\}}{\{\text{SO}^{(z_2+1)-}\}[\text{H}^+]^{\text{int}}} \quad (27)$$

and the corresponding expression for the surface potential is:

$$\psi_0 = \frac{k_B T}{e} \ln \left[\frac{z_1 \theta_{z_1} + z_2 \theta_{z_2}}{(1-z_1)\theta_{z_1} K_1 + (1-z_2)\theta_{z_2} K_2} \right] - \frac{2.303 k_B T}{e} \text{pH} \quad (28)$$

where $\theta_{z_1}, \theta_{z_2}$ represent the fractional surface occupations of the empty (negatively charged) sites with charges z_1 and z_2 , respectively.

Because the surface concentrations of individual ions are rarely available, these definitions (Equations (16,20,27)) are of limited experimental use in practice. However, they allow us explain the deviation of ψ_0 from ideal Nernstian behavior as the consequence of surface complexation and protonations reactions.

In principle, the surface electrostatic response of nonpolarizable electrodes can be defined as the ideal Nernstian behavior ($\alpha = 1$) decreased by the term $\psi_0(\theta)$ (containing all surface protonation/complexation processes):³⁰

$$\psi_0^{\text{quasi-Nernst}}(\text{pH}) = \alpha \psi_0^{\text{Nernst}}(\text{pH}) = \psi_0^{\text{Nernst}}(\text{pH}) - \psi_0(\theta) \quad (29)$$

Computer Simulation of the Surface Potential: Monte Carlo Lattice Model

One of the most popular computational methods in adsorption science is numerical simulation of a lattice surface model, which is an adaptation of the Ising model of a ferromagnetic material for solid/(liquid/gas) interfaces.^{39,40} For years it has been used as a numerical tool in testing analytical theories (*e.g.*, to simulate adsorption isotherms and surface phase transitions).^{39,40} To a certain extent, this simulation method can be viewed as a computer experiment.⁴¹ This approach has nonetheless provided very useful and unique insight into microscopic chemical and physical phenomena behind macroscopic behavior. In particular, lattice models can be tailored to a desired configuration to enable simultaneous development of analytical theoretical models. And in particular, strengths of this approach include computational efficiency, and the ability to switch elementary processes in the system on/off depending on the model requirements, a feature that enables study of, for example, the effects of individual microscopic processes on macroscopic thermodynamic observables.

A numeric lattice model description of the metal oxide/electrolyte interface was introduced by Borkovec and coworkers.^{42,43} In its original formulation, the Borkovec model includes only the uptake/release of surface H^+ ions on a simple surface lattice as the primary source

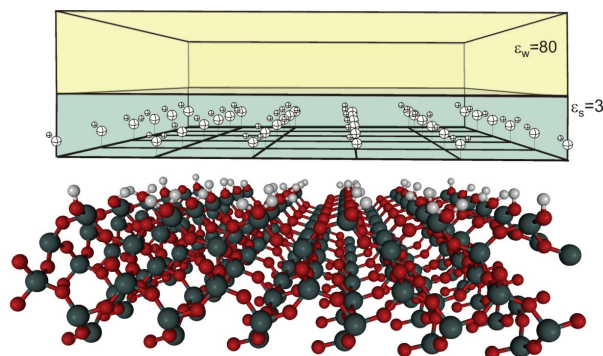


Figure 3. Lattice model of electrical interfacial layer formed at the metal oxide/electrolyte interface used for Grand-Canonical Monte Carlo and Kinetic Monte Carlo simulations (see References 30, 31, 34, 44–50). The two continuum dielectric regions are used to describe the interface and bulk phase, with dielectric constants ϵ_s and ϵ_w , respectively.

of surface charge.^{42,43} This approach includes use of a pair-wise electrostatic interaction potential between charged surface groups, with the effect of intervening electrolyte treated in a mean-field way by using Debye screening. We have expanded this model by including effects of surface energetic⁴⁴ or topographic nonuniformity, as well as by expanding to the cellular Potts model analog to study the effect of electrolyte ion surface association.^{45,46} In our studies, equilibrium properties were obtained using Grand Canonical Monte Carlo algorithm,^{44–46} whereas kinetic ones were obtained by using the Grand Canonical Kinetic Monte Carlo method.^{47,48} A basic model lattice we have used in combination with the Borkovec interaction potential to simulate the metal oxide/electrolyte interface is schematically presented in Figure 3. Although this approach seems very simple, it has proven to be a valuable tool for using microscopic principles to test the validity of popular surface analytical models, such as ones that are based on the integral adsorption isotherm approach.^{44,49} Furthermore, because individual adsorption isotherms are direct observables in lattice Monte Carlo simulation, we can evaluate the equilibrium surface potential by employing appropriate formula (*e.g.*, from Equations (16,20,24,27)).^{30,34} More detailed description of these simulations and their utility for metal oxide/electrolyte interfaces can be found in our previous papers.^{30,34,47–50}

Computer simulation of the surface potential: Molecular dynamics

Molecular dynamics, a widely used atomistic simulation method that depends heavily on the accuracy of empirically derived interatomic interaction potentials, allows study of both equilibrium and kinetic properties of a metal oxide/electrolyte interfacial system. However, this approach is in general more computationally intensive

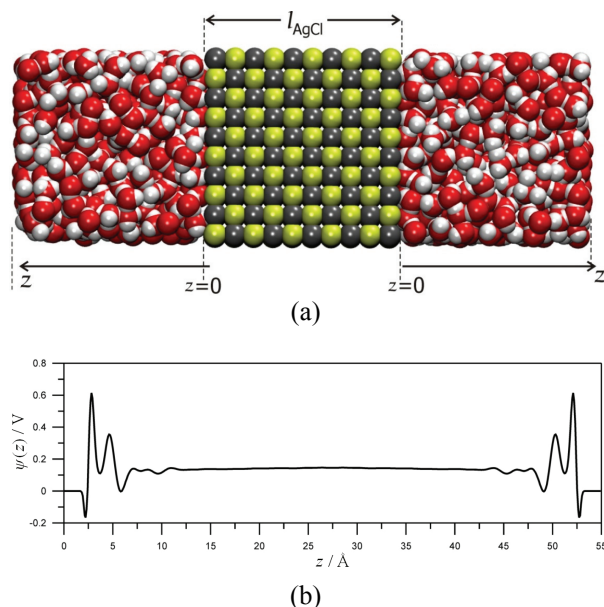


Figure 4. (a) simulation cell used in estimating electrostatic properties of AgCl/electrolyte interfaces using molecular dynamics simulations; (b) The electrostatic potential between both solid planes calculated for the AgCl/KCl_(aq) electrolyte system periodically replicated in each direction. The details of the molecular dynamics calculations can be found in References 56 and 57.

than in the Monte Carlo lattice model approach and therefore can suffer from inability to reach into long time scales (*e.g.*, greater than a few tens or hundreds of nanoseconds) or very large system sizes (*e.g.*, to simulate low electrolyte concentration). Furthermore, incorporation of a chemical reaction, which entails bond making and bond breaking events, is much more difficult than in a Monte Carlo lattice approach. Aspects of the difficulty lie in the ambiguity of defining universal criteria for when specific bonds are formed or broken, and avoiding discontinuities in the potential energy surface when such events are specified to occur. Therefore, in a molecular dynamics simulation of the interface, chemical entities are usually restricted to remain unchanged as the system dynamics evolve. To our best knowledge, for metal oxide surfaces and their interfaces with aqueous solution, there is currently only one molecular dynamics model that has successfully incorporated water dissociation.^{51,52} For these reasons, use of molecular dynamics simulation to analyze metal oxide surface electrostatic properties as a function of pH is very limited. There are, however, numerous studies of hydrated metal oxides using non-dissociable water models (*e.g.*, References (53–55)), which can provide some insight into the distribution of charge/ions across the interface.

Fortunately, in the case of the silver halide/electrolyte interfaces, water molecules can be treated as

inert solvent, and the halide or silver ions play the role of PDIs. In Figure 4 we show a molecular dynamics simulation model recently used to calculate electrostatic properties of the AgCl(100)/KCl_(aq) (0.24 mol/dm³) interface, along with the calculated electrostatic potential profile.^{56,57} As shown in Figure 4, the simulation cell in this instance is composed of the crystal slab and the electrolyte phase periodically replicated in three dimensions. The electrostatic potential profile is obtained by a double integration of the ion and water charge density curves:^{60–65}

$$\psi(z) = -\frac{1}{\epsilon_0} \int_0^z \int_0^z \sigma(\zeta) d\zeta \quad (30)$$

where ϵ_0 is the dielectric permittivity of free space, z is the distance from the surface ($z = 0$) into the bulk electrolyte phase and ζ represents the integration variable (distance).

CHALLENGES

Determination of Surface Potential Using a Single-Crystal Electrode

As mentioned above, in order to convert the measured electromotive force of the cell based on a single-crystal electrode to the surface potential, the voltage shift (E_T , see Equation (5)) has to be known in advance. The simplest way to assess E_T is based on the requirement that surface potential at pH = PZC is equal zero. If the PZC of a given crystal face exposed to the electrolyte was known, in principle one could simply set $E_T = E(\text{PZC})$. Unfortunately, the PZC of individual crystal faces are largely unavailable. It is much more common to have only either the PZC or IEP from batch potentiometric titration or electrophoretic measurements on powder metal oxide particulates, typically of unknown or unspecified crystallite morphologies.⁶⁶ In both experimental procedures, because a metal oxide suspension is used,⁶⁷ the determined PZC/IEP represents is an average of numerous surfaces and types of surface sites (different crystal faces, terminations, edges, kinks, defects). Hence, use of this average characteristic for shifting the cell voltage for a SCrE setup is dubious. Furthermore, an estimation of the potential slope (α) is available directly from SCrE measurements, and it does not require prior knowledge of PZC.

Although in general there is no a priori knowledge of the PZC of a single crystal face, one can try to estimate it based on the presumed or measured stoichiometry of the exposed crystal face using the MUSIC or CD-MUSIC surface complexation models.^{37,38} However, in practice this still requires an unsatisfying number of assumptions to be made about the surface termination

and its level of compositional and structural perfection, and the activity of different surface sites. The estimated PZC will therefore be strongly model-dependent.

In some of the first uses of an SCrE, the value of E_T was approximated using the PZC or IEP obtained for the powdered metal oxides. However, recently we introduced a novel approach for estimating the PZC of individual crystal faces based on the observation that in SCrE measurements involving sequential forward and reverse pH titration typically one finds reproducible hysteresis in the measured cell potential as a function of pH. This phenomenon was first reported for the case of a single-crystal hematite electrode by Preočanin and Kallay.¹⁸ A similar hysteresis loop has also been observed in batch potentiometric titration⁶⁸ and calorimetric measurements.⁶⁹ The kinetic character of hysteresis was immediately recognized: by extending the titration time or applying ultrasound mixing the hysteresis separating the acidimetric and alkalimetric titration branches could be reduced.¹⁸ If no steps are taken to reduce the hysteresis, one is left with the conclusion that in the region of separated branches the SCrE surface is undergoing overcharging in the alkalimetric titration (overpotential- slightly higher potential than we should observe at the equilibrium), and undercharging during the acidimetric titration (underpotential). Surface overcharging (overpotential) is a manifestation of the fact that not all surface protons were able to leave the surface before another aliquot of base was added (with respect to equilibrium). Conversely, surface undercharging (underpotential) is evidence that not all protons were able to be bound to the surface before another aliquot of acid was added.⁷⁰

Given this behavior, the difference in measured potential between the acidimetric (ba, basic to acidic pH) and alkalimetric (ab, acidic to basic pH) titration branches gives the free energy difference between both titration curves:

$$\Delta E = E^{ab} - E^{ba} = -\frac{1}{eN}(\Delta G^{ab} - \Delta G^{ba}) = \psi_0^{ab} - \psi_0^{ba} \quad (31)$$

Therefore, under this condition, the cell, in which the overall cell reaction has not yet reached equilibrium, can do electrical work.^{8,9} Furthermore, as is the case in magnetic hysteresis phenomena, the area enclosed by the hysteresis loop is the work done on the system.⁷¹ The difference (ΔE , Equation (31)) approaches zero as the titration time is extended and the system is allowed sufficient time to reach equilibrium at each pH value. In principle, one should be able to find a pH value at which over/undercharging of the positively charged surface has the same free energy as over/undercharging of the negatively charged surface. This pH value should roughly estimate the pH of electrostatic metastability of the cell, and should be identical to the pH value corres-

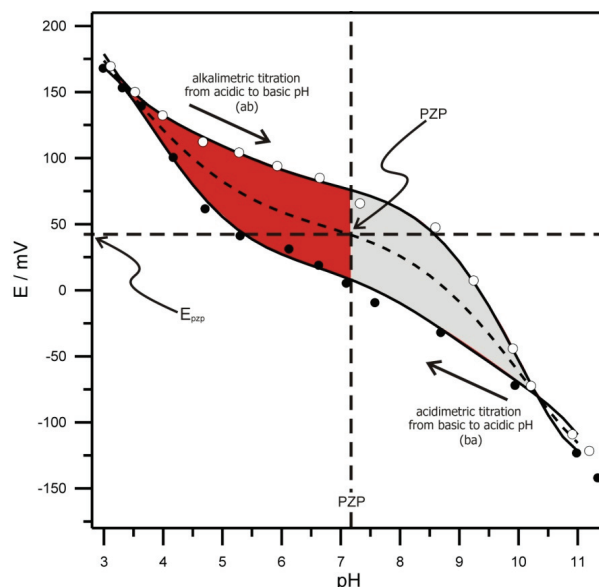


Figure 5. A measured titration hysteresis loop obtained using single-crystal electrode measurements (markers) (hematite 021/0.001 mol/dm³ NaNO₃). By adapting the concept of the Maxwell construction to the problem of titration hysteresis, we can estimate the surface PZC value and shift in cell potential ($E_{pzp} = E_T$) as equal to 7.2, and 35 mV, respectively. The experimental and numerical details can be found in Reference 70.

ponding to the PZC of the fully equilibrated system. Based on the theory of the ferromagnetic hysteresis, we found that this zero potential condition (pH = PZP) can be found using the Maxwell construction of an equal area. The pH = PZP corresponds to the vertical plane (pH = ζ) which divides hysteresis into two equal areas (see Reference 70 for more details):

$$I(\zeta) = \int_{\text{pH}_{\text{start}}}^{\zeta} \Delta E(\text{pH}) d\text{pH} - \int_{\zeta}^{\text{pH}_{\text{end}}} \Delta E(\text{pH}) d\text{pH} \quad (32)$$

where $\Delta E = E^{ab} - E^{ba}$

Application of this procedure is illustrated for experimental data obtained for hematite(021)/0.001 mol/dm³ NaClO₄ electrolyte solution in Figure 5 (data from Reference 70). This procedure therefore allows us to determine the PZC of individual crystal faces directly from the titration experiment. Such an analysis provides unique insight into the acid-base response of metal oxide surfaces not afforded by other surface spectroscopic probes. In principle, with knowledge of the surface structure, it enables one to estimate protonation constants of individual crystal faces from experiment for the first time. For a more detailed description of this approach, see Reference 70.

Another way of estimating the surface PZP is based on analogy to Gran plots used in potentiometric selective electrode titration.⁹ If high resolution cell po-

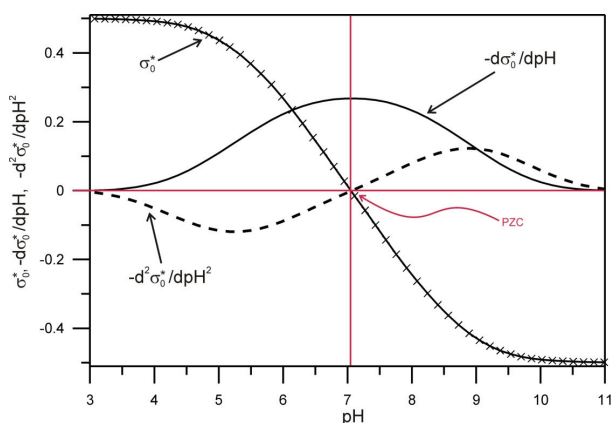


Figure 6. Theoretical surface charge density curve ($\sigma_0^* = f(\text{pH})$) and its first ($-d\sigma_0^*/d\text{pH}$) and second derivatives ($-d^2\sigma_0^*/d\text{pH}^2$) with respect to pH. The $\text{pH} = \text{PZC}$ is an inflection point of the charging curve. Results were obtained using Grand Canonical Monte Carlo simulations of a lattice model (see Reference 70 for details).

tential measurement can be achieved (*i.e.*, the ability to collect a large number of $E = f(\text{pH})$ points), the PZP can be estimated by using numerical derivative ($dE/d\text{pH}$). It has been experimentally proved using high resolution potentiometric titration,^{72,73} and Monte Carlo simulation (Figure 6) that the surface charging curve possess an inflection point at the $\text{pH} = \text{PZC}$. An analogous property can be expected from the surface potential curve, that is, the maximum of the $dE/d\text{pH}$ curve should coincide with the PZP (and $d^2E/d\text{pH}^2 = 0$ at $\text{pH} = \text{PZP}$). There are two major obstacles to this approach in practice. First, as already mentioned, the typical potential measurement shows a hysteresis loop which obscures the correct inflection point. It is also possible at times to obtain an essentially linear profile, which results in a constant value of $dE/d\text{pH}$ (each point will be an inflection point). Secondly, current experimental methods typically do not allow one to collect sufficiently high-resolution data to obtain a reliable derivative of the cell potential with respect to pH. Hence this method is somewhat relegated to systems in which hysteresis can be eliminated and where experimental capabilities are uniquely capable for this application.

Nonlinear Single-crystal Electrode Response

In the surface complexation community, there is a strong belief that surface potential should be a linear function of potential determining ion concentration at the surface ($\psi_0 \approx \text{pH}$). This is understandable given that the metal oxides represent one kind of nonpolarizable surface, which in general is expected to obey the Nernst equation (*e.g.*, similar to the Ag|AgCl reference electrode). Early measurements based on the ISFET electrode confirmed the expected linearity of surface poten-

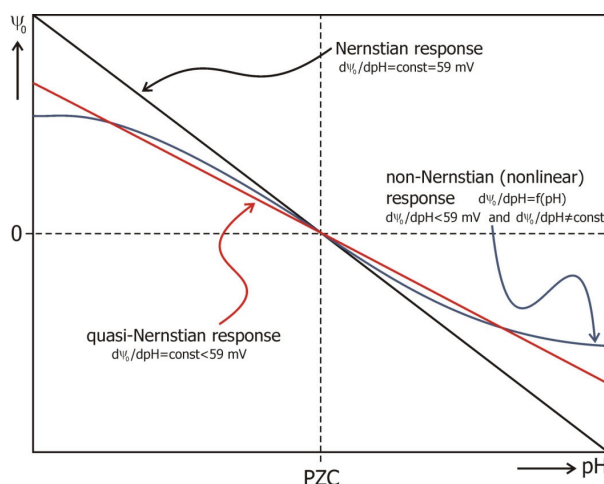


Figure 7. Types of surface potential response to the change in potential determining ions (here H^+ ions): (i) Nernstian response, expected for the ideally nonpolarizable electrode (*e.g.*, Ag|AgCl), (ii) quasi-Nernst, expected for metal (hydr)oxide/electrolyte interfaces (linear function of pH, but lower than Nernstian slope), (iii) non-Nernstian (or non-linear) behavior, where the slope of the response is not constant and varies with the bulk pH.

tial as a function of pH, and also proved that the actual electrode response is somewhat of lower slope than predicted by the Nernst equation (Equation (7)). As mentioned before, this lower slope in the relationship is quantitatively described by the α parameter in the quasi-Nernst equation (Equation (10)). However, recently the expectation of linear electrostatic response for metal oxide electrodes has started to be questioned on grounds that at a fundamental level these surfaces are typically structurally and compositionally irregular.³⁰ This gives rise to many possible sources of nonlinearity; one of the most striking is the coupling of electrostatic effects and surface morphology. A distribution of possible ion/proton affinity constants (*i.e.*, a spectrum of adsorption energies) arises from the fact that at the atomic scale, metal oxide surfaces are generally defective, with the potential to deviate substantially from ideal crystallographic terminations. Although it has also been found that, to some extent, long-range electrostatic interaction between surface sites couples with structural reconstruction/relaxation to smooth an initially rough surface (*e.g.*, one possible mechanism of surface free energy minimization), an energetic spectrum of surface adsorption energies nonetheless remains from one termination to the next. Hence, at any particular metal oxide surface, the ensemble of surface sites should be considered to be in a state of dynamic equilibrium with each other. In some cases this dynamic equilibrium appears to extend even further to intersurface interaction. For example, Yanina and Rosso⁷⁴ showed near-macroscopic scale evidence that net structural distinction between surfaces

of a hematite crystal is sufficient to couple oxidative deposition of ferrous iron at one surface type to reductive dissolution of ferric iron at another surface type, mediated by transfer of electrical current through the crystal bulk. The thermally activated self-diffusion of electrons (*i.e.*, as small polarons) through the crystal is sufficient to allow multiple exposed crystal faces to remain in electrostatic contact and as a result induce dissolution of one and growth of another.⁷⁴ Such inter-surface interaction warrants further investigation with respect to its role in influencing the surface potential at any particular surface of a whole crystal exposed to electrolyte solution.

For SCrE measurements, it turns out that the typical $\psi_0 = f(\text{pH})$ profile is only rarely a linear function. Representative Nernstian, quasi-Nernstian and non-Nernstian (*i.e.*, nonlinear) surface potential responses are illustrated in Figure 7. In past practice, the linearity of surface potential has required that the parameter α is independent of pH, that is:

$$\frac{d\alpha}{d\text{pH}} = 0, \quad \frac{d^2\psi_0}{d\text{pH}^2} = 0, \quad \text{or} \quad \frac{d^2\Delta G}{d\text{pH}^2} = 0 \quad (33)$$

The linearity can be analyzed by plotting $\alpha = f(\text{pH})$, as already suggested by Bousse *et al.*¹⁰ In addition, earlier we compared SCM expressions for the surface potential (Equations (16,20,24,27)) with a quasi-Nernst one (Equation (10)) and were able to re-express α as a function of fractional surface coverage (Equations (17,21,25)). An outcome is that these expressions show that the slope of depends on the adsorption progress, and can be expected to vary with pH (Equation (29)). A limitation is the fact that α is composed somewhat differently in each expression and the choice of which form to apply remains somewhat arbitrary.

To deal with this issue, we recently proposed a new way of analyzing surface potential nonlinearity, based on perturbative expansion of the free energy with respect to reduced pH units ($\zeta = \text{PZC} - \text{pH}$).³⁰ By considering an idealized Nernstian electrode as a reference system (unperturbed), we introduce terms for both deviation from Nernstian behavior as well as the deviation from linearity as perturbations:³⁰

$$\psi_0 = \frac{2.303k_{\text{B}}T}{e} \sum_{i=1} \alpha_i \zeta^i \quad (34)$$

If the expansion is truncated after $i = 1$, then we obtain the quasi-Nernst equation (Equation (10)). In principle, all higher terms in the expansion (*i.e.*, $(k_{\text{B}}T/(ne))\alpha_i \zeta^i$ for $i > 1$) have the meaning of perturbative corrections to the linear quasi-Nernst equation. Based on computer simulation results, we found that the magnitudes of the expansion coefficients ($|\alpha_i|$) decrease with

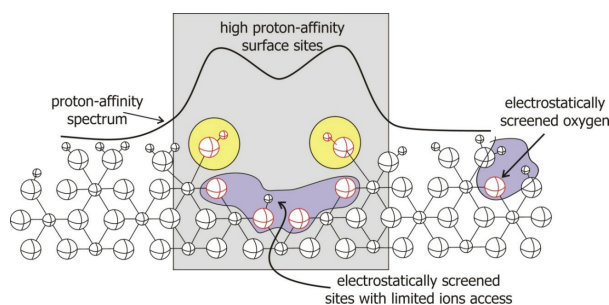


Figure 8. Schematic illustration of electrostatic screening at sterically constrained surface sites on energetically/topographically rough surfaces. Surface sites exposed on the edges and kinks are in energetically excited states that relax through proton adsorption, ion complexation, and local geometric relaxation. However, long-range electrostatic repulsion between adsorbed ions/protons can still be present and can prevent some surface sites from relaxing via adsorption.

order (*i*). In principle, they depend on the source of nonlinearity, for example, arising from surface heterogeneity or surface phase transformations and/or accompanying reactions. However, application of Equation (34) to experimental data awaits the availability of higher resolution SCrE surface potential measurements.

The relationship between nonlinear electrode response and surface heterogeneity deserves further discussion.³⁰ Surface heterogeneity so far has been discussed in terms of coupled structural and chemical surface complexity; a natural convolution of topographic variability yielding a broad range of adsorption energies for PDIs. Here for the purposes of illustrating separate effects via computer simulation, we can discuss an operative distinction between pure topographic surface heterogeneity involving only surface roughness and structurally distinct surface sites having differences limited in scope to geometric variability in physical access and intersite electrostatic interaction, and pure energetic surface heterogeneity involving a discrete or continuous spectrum of PDI adsorption energies alone without ties to surface topography (*i.e.*, on a flat surface). It has been already shown that surface energetic heterogeneity has a tremendous effect on acid-base properties of metal oxide/electrolyte interfaces.^{44–50} Energetic heterogeneity is considered in lattice models by assuming a discrete/continuous spectrum of PDI adsorption energies (proton and ion affinity constants).^{44–50} Perhaps more complicated is the separate role of topographic heterogeneity. We recently showed that topographic heterogeneity, and any associated local variation in intrinsic affinity, can be effectively screened by electrostatic interaction.⁵⁰ As illustrated by Figure 8, even in the event that neighboring sites both possess strong proton affinity, the occupation of one site can prevent the neighboring one from being occupied due to electrostatic repulsion. Hence because site-to-site elec-

trostatic forces are of a longer range than chemical ones they can dominate the local site reactivity. As already mentioned, because it naturally is convoluted with site reactivity, this effect is strong enough to help reduce surface roughness through dynamic restructuring of the surface.⁴⁵ In particular, this phenomenon needs to be taken into account in any attempt to project the topographic heterogeneity studied in the gas-phase to charged interfaces in aqueous solution (*e.g.*, the surface area determined by BET adsorption isotherm analysis does necessarily correspond to the actual surface area when in contact with an aqueous phase).

Although energetic heterogeneity is a well justified and accepted characteristic of powder metal oxide particulates, its applicability is less immediately clear in the case of an SCrE electrode. However, even though a single-crystal electrode is typically designed to expose only a single crystal face, it is often then required to endure prolonged contact with aqueous solution. The high reactivity of freshly cleaved or otherwise dry prepared oxide surfaces toward water (*e.g.*, to water chemisorption at very low partial pressure) has already reported.⁷⁵ Progressive surface relaxation/reconstruction processes can thus occur to reduce the surface free energy, yielding a fundamentally different termination of the selected crystal face. It is also possible that an energetically more stable face forms by deposition on the top of the original one. This dynamic phenomena can result in surface roughening or amorphization, particularly if the electrode is extensively exposed to pH extremes. The likelihood of all such phenomena suggest that the most reliable ψ_0 -measurement possible requires that the measurements be accompanied by careful electrode surface monitoring (*e.g.*, by using scanning probe microscopic techniques).

We end this section by noting a key area for future work. In most cases for metal oxide/electrolyte interfaces the interfacial charge is developed exclusively on the metal oxide surface and any redistribution of charge within the solid itself neglected. However, in the case of semiconducting metal oxides, the space-charge region can be neglected only at certain value of the applied potential, at which the number of electrons removed and supplied to electrode is equal.⁹ If this is not the case, there is additional potential drop within the space-charge region, with a finite capacity (*i.e.*, the Mott-Schottky capacity).⁹ This capacity is usually a linear function of applied potential, but nonlinearity appears if there are adsorbed species on semiconductor surface.⁹ Moreover, the presence of the electrical interfacial layer results in another Schottky barrier formation at the semiconductor/electrolyte interface. These potential jumps are presently neglected in the Surface Complexation Modeling approach but warrant further investigation.

Specific Adsorption

As mentioned above, in order to simplify the notation we assumed a lack of specific ion adsorption (*i.e.*, similar affinities of electrolyte ions), which allowed us to write all equations using only the point of zero charge. However, specific ion adsorption has been frequently invoked to explain the data from SCrE measurements,^{21,66} and it therefore is advisable to use the term point of zero potential (PZP) while discussing pH at which $\psi_0 = 0$.^{21,66} By specific adsorption we mean that in the accumulation of a particular ion at the surface the formation of chemical bonds is involved. The formation of an electrical interfacial layer in the absence of specific adsorption is driven by the electrostatic interactions, and thus the variation in ionic strength should not affect the point of zero charge. In this case, at $\text{pH} < \text{PZC}$ the surface is positively charged and anion adsorption dominates, whereas at $\text{pH} > \text{PZC}$ the surface is negatively charged and cation adsorption dominates. If specific adsorption occurs, chemical bonding forces are also involved and ion-surface interactions can be strong enough to overcome electrostatic repulsion (*e.g.*, anions can accumulate at a negatively charged surface: $\text{pH} > \text{PZP}$, $\psi_0 < 0$, or cations at $\text{pH} < \text{PZP}$, $\psi_0 > 0$). Specific adsorption is usually detected by looking at the dependence of the PZC and/or IEP on the ionic strength:

$$\frac{d\text{PZC}}{dI} \neq 0 \quad \text{and} \quad \frac{d\text{IEP}}{dI} \neq 0 \quad (35)$$

Because specific adsorption varies with electrolyte concentration, the positions of the PZC and IEP depend on ionic strength. This is a known as the Esin-Markov effect and it is commonly encountered at metal/electrolyte interfaces.⁹ Quantitative description of the PZC dependence on specific adsorption is provided by the Esin-Markov coefficient (β_{EM}):⁹

$$\beta_{\text{EM}} = \frac{1}{k_{\text{B}}T} \frac{d\text{PZC}}{d \ln c} \quad (36)$$

In the case of symmetric ion adsorption (*e.g.*, electrostatically driven complexation) we observe an equal adsorption of electrolyte ions at $\text{pH} = \text{PZC}$ (*e.g.*, within the 1-pK model: $[\text{SOH}_2^{1/2+} \text{A}^-] = [\text{SOH}_2^{1/2-} \text{C}^+]$) and consequently self-balancing of protonated/deprotonated sites (*e.g.*, within the 1-pK model: $[\text{SOH}_2^{1/2+}] = [\text{SOH}_2^{1/2-}]$). In this instance, the concentration of surface complexed ions increases with ionic strength, but due to the equality in their relative amounts at the PZC, the position of the point of zero charge remains independent of the electrolyte concentration.

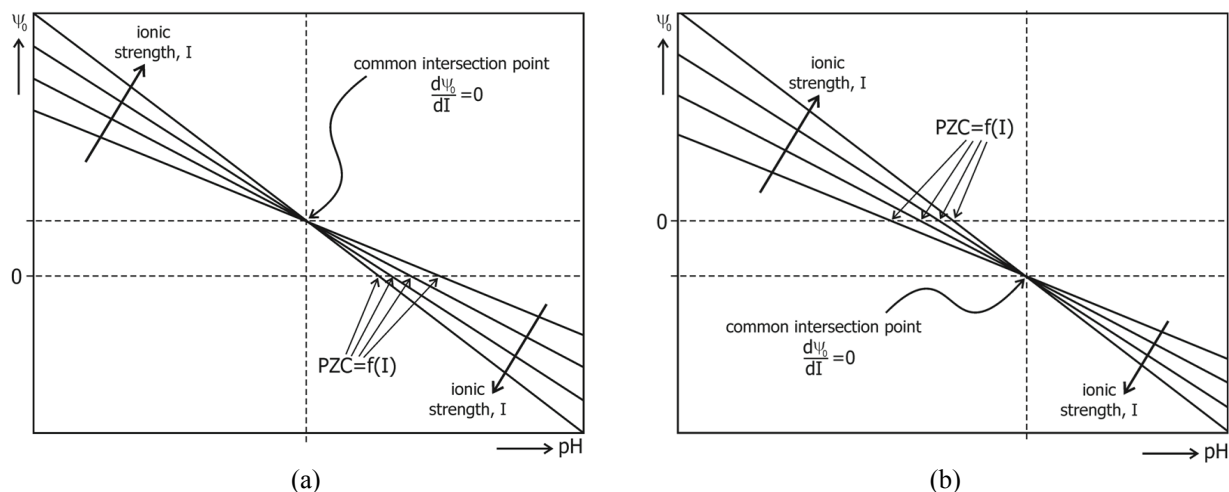


Figure 9. The dependence of surface potential on ionic strength in the case of cation (a) and anion (b) preferential adsorption. The shift in PZC with ionic strength and the relative position of the common intersection point (CIP) also known as the point of zero salt effect are schematically presented.

In the case of preferential cation adsorption we observe a higher surface concentration of adsorbed cations than anions at $\text{pH}=\text{PZC}$ (within the 1-pK model: $[\text{SOH}_2^{1/2+}\text{A}^-] < [\text{SOH}_2^{1/2-}\text{C}^+]$). This discrepancy in ion surface concentration increases with increasing ionic strength. Because the cations are bound to the deprotonated groups ($\text{SOH}^{1/2-}$ in 1-pK) they effectively contribute negative charge to the surface charge/potential. The protonation balance therefore has to be shifted toward increasing concentration of $\text{SOH}_2^{1/2+}$ groups to maintain the overall surface neutrality, and consequently the PZC is shifted towards lower pH values (shift increases with an increase in ionic strength). At the point in which surface concentrations of electrolyte ions are equal (*i.e.*, in 1-pK model: $[\text{SOH}_2^{1/2+}\text{A}^-] = [\text{SOH}_2^{1/2-}\text{C}^+]$) the titration curves intersect. This pH value is called the common intersection point (CIP) or point of zero salt effect (PZSE).³² In the case of preferential cation adsorption, the CIP can be achieved if anion adsorption is facilitated by electrostatic attraction (*i.e.*, the CIP is located at $\text{pH} < \text{PZC}$). This case is illustrated in Figure 9a.

The opposite situation is observed if anions are preferentially adsorbed. In this case, at $\text{pH} = \text{PZC}$ we observe a higher surface concentration of adsorbed anions than cations (*i.e.*, in the 1-pK model: $[\text{SOH}_2^{1/2+}\text{A}^-] > [\text{SOH}_2^{1/2-}\text{C}^+]$). Because, the adsorbed anions effectively contribute positive charge to the surface potential, to reach surface electroneutrality deprotonated sites have to balance the complexed anions and protonated sites. The PZC therefore shifts towards higher pH values, and this shift is also directly proportional to the ionic strength. The equality of surface concentration of complexed electrolyte ions can be obtained if cation adsorption is enhanced by the electrostatic attraction, and consequently the CIP is

observed at $\text{pH} > \text{PZC}$ (at $\psi_0 < 0$). This situation is depicted in Figure 9b.

Specific ion adsorption is observed only rarely in a potentiometric titration experiment, and it is usually treated as an anomaly of the more commonly observed zero salt effect (see Reference 76 and references therein). For instance, Cs^+ ions are found to be preferentially adsorbed on anatase,^{76,77} with the CIP at $\text{pH} < \text{PZC}$ ($\sigma_0 = 0.2 \mu\text{C}/\text{cm}^2$). Similarly, complexation of Li^+ on hematite⁷⁸ is driven by specific adsorption. Preferential adsorption of NO_3^- ions on Al_2O_3 , with the CIP at $\text{pH} > \text{PZC}$ ($\sigma_0 \cong -3.5 \mu\text{C}/\text{cm}^2$)⁷⁹ serves as an illustration of anion specific adsorption.

Contrary to potentiometric titration experiments of metal oxide suspensions, specific ion adsorption seems to be frequently observed in SCrE measurements.⁸⁰ One can deduce from this that this is evidence of the compensation effect of simultaneous exposure of many crystal faces in the former approach. The single-crystal electrode can detect specific adsorption undetected by surface charge/ ζ -potential measurements on suspensions, which also calls into question the use of the IEP or PZC to transform measured cell potential into surface potential. In summary, a single-crystal electrode method is very sensitive in tracing the acid-base properties of metal oxide surfaces, and all things considered it seems to emerge superior to electrokinetic/potentiometric titration experiments on suspensions.

Electron Transfer

Redox processes at the metal oxide surface can be also considered as the source of a nonlinear metal oxide electrode response. Electron transfer is a Franck-Condon process, which means that charge transfer

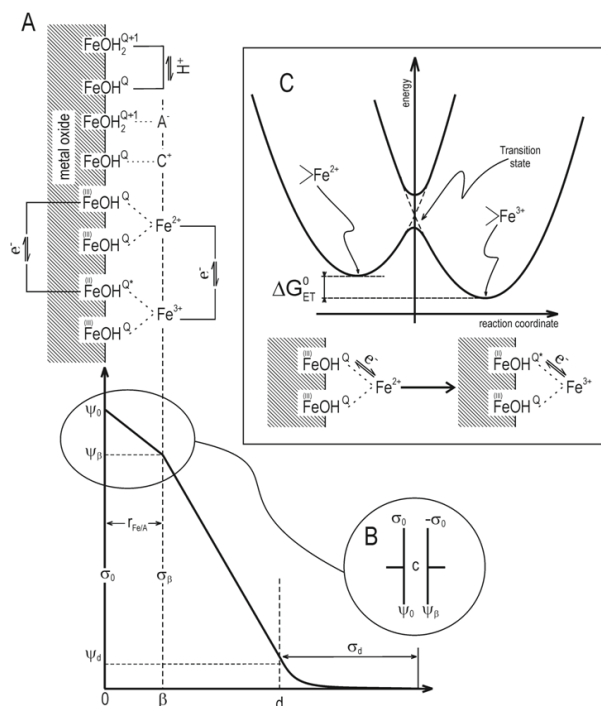


Figure 10. Surface complexation model combined with an adiabatic interfacial electron transfer event (example for Fe^{2+} ion adsorption at the goethite/electrolyte interface (see Reference 83)).

occurs fast compared to the timescale of nuclear fluctuations, and therefore occurs without affecting the nuclear degrees of freedom.⁸¹ However, prior to the actual charge transfer, the nuclear configuration of donor and acceptor have to reach a transition state geometry at which the electronic states of the donor and acceptor are energetically degenerate.⁸² In the case of metal oxides, the electron transfer is typically an adiabatic process, that is, there is strong electronic coupling between donor and acceptor wavefunctions at the transition state geometry, which substantially decreases the electron transfer energetic barrier (Figure 10). The rate of adiabatic electron transfer can be described using the classical Arrhenius formalism, hence electron transfer can be considered in the simplest sense as an additional reaction in Surface Complexation Models (see Figure 10).⁸³ We are currently developing an analytical version of such a model which includes the possibility of adiabatic electron transfer events.⁸³ The accompanying change in the surface site oxidation state affects the surface charge and potential, and in principle this is can be detected by a single crystal electrode measurement (see References 74 and 87).

Molecular-level insight into such electron transfer process can be obtained using computational molecular

simulation methods, in particular the umbrella sampling technique developed by Warshel and coworkers.⁸⁵ In Figure 11, we show simulation results for $\text{Fe}(\text{II})$ interfacial electron transfer with $\text{Fe}(\text{III})$ in the (101) surface of goethite in contact with aqueous solution. In Panel A, the calculation of potential of mean force for the approach of $\text{Fe}(\text{II})$ to the surface is used to identify stable inner/outer surface complexes of adsorbed $\text{Fe}(\text{II})$, whereas in panel B the energetics of electron transfer in an inner-sphere configuration and within the mineral subsurface region are presented. More detailed discussion can be found in our recent paper.⁸⁶

CONCLUSIONS

In this feature article, we summarized current experimental, theoretical, computational methods for analyzing and understanding the electrostatic potential at single-crystal electrodes of metal (hydr)oxides. Substantial progress has been made in use of single-crystal electrodes as a tool for understanding fundamental chemical and physical processes governing the electrostatic potential distribution across metal (hydr)oxide/electrolyte interfaces, but challenges remain. Improvements in the design of single-crystal electrodes are still under development. Here we have overviewed some of the present difficulties and have suggested solutions. One of them is to make use of the hysteresis observed in cyclic titration experiments to directly estimate the point of zero potential for a well-defined single-crystal face. Analysis of evaluated ψ_0 -profiles is also a difficult task, and many second order processes can contribute to non-Nernstian behavior. In particular, the surface roughness/recrystallization, redox reactions, specific adsorption and unrecognized potential jumps across the interface have to be better understood, quantified, and taken into account. The experimental procedure indeed requires more extensive study, and the various experimental/theoretical procedures outlined herein are currently being refined and tested between Kevin M. Rosso's and Nikola Kallay's research teams.

Acknowledgements. This work was supported by the grant from the US Department of Energy, Office of Basic Energy Sciences, Geosciences Program. The research was performed using EMSL, a national scientific user facility, sponsored by the Department of Energy's Office of Biological and Environmental Research located at Pacific Northwest National Laboratory. Tajana Preočanin and Nikola Kallay were supported by the Ministry of Science, Education and Sports of the Republic of Croatia (Project No. 119-1191342-2961).

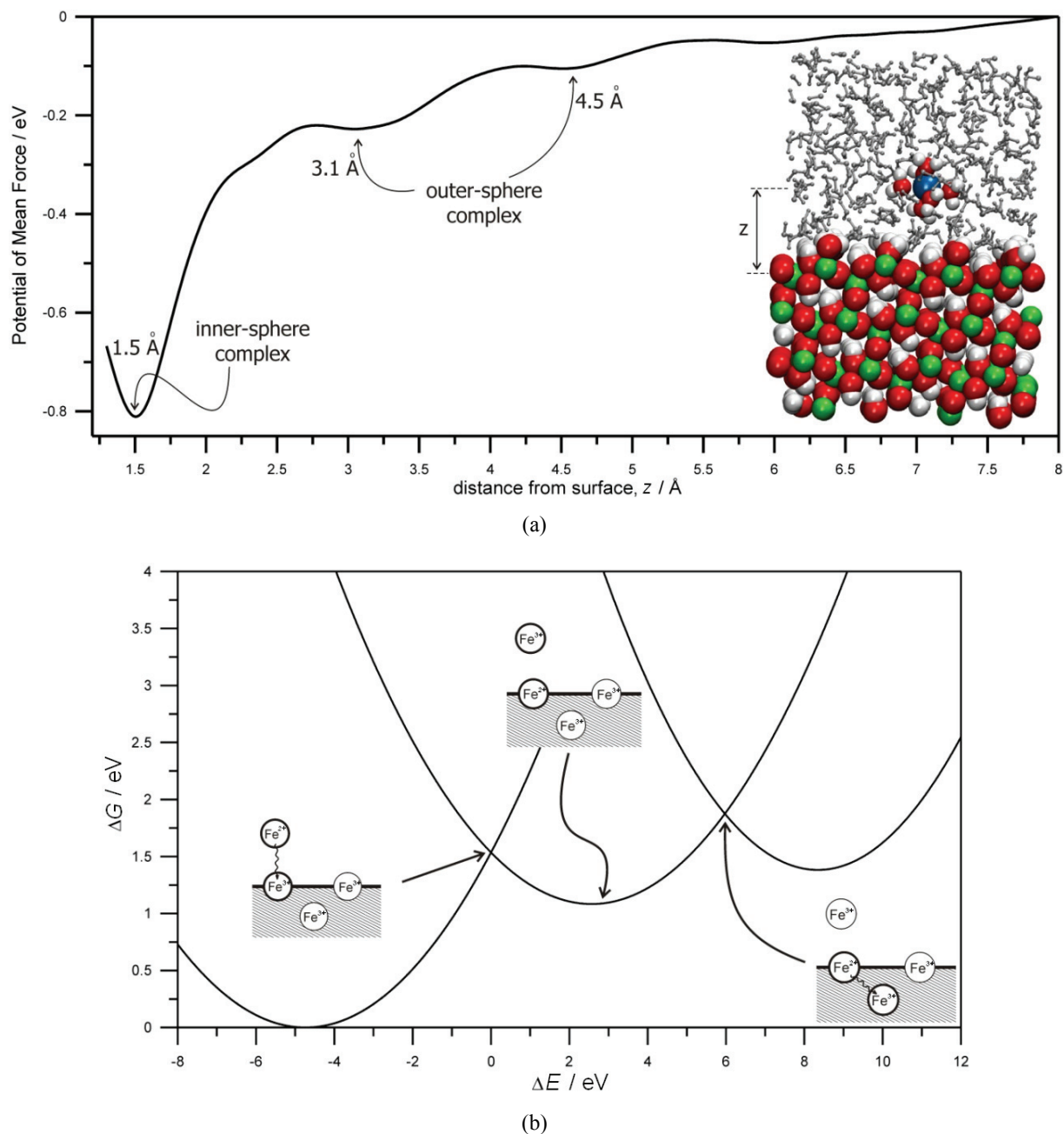


Figure 11. Molecular dynamics study of electron transfer across the goethite 101/electrolyte interface and into the solid. The potential of mean force (a) enables identification of possible inner and outer-sphere complexes. Free energy profiles (b) were obtained using the umbrella sampling technique (for details see Reference 85).

Glossary

E	potential of the cell
E^{SCrE}	the absolute potential of the Single-Crystal electrode
E^{ref}	the absolute potential of the reference electrode
V	additional voltage drop due to formation of electrical interfacial layer
i	electric current caused by the formation of electrical interfacial layer
R	Ohmic resistance due to formation of the electrical interfacial layer
$\Delta \phi^{\text{SCr/sol}}$	the Galvani potential at the single crystal/electrolyte interface

(continued)

$\Delta \phi^{\text{ref/sol}}$	the Galvani potential at the reference/electrolyte interface
$\mu_i^{\text{Scr/sol}}$	chemical potential of potential determining ions near the Single Crystal Electrode
$\mu_i^{\text{ref/sol}}$	chemical potential of potential determining ions near the reference electrode
C	constant shift in measured cell potential. It represents all potential jumps within the cell which do not depend on the concentration of potential determining ions
χ^{SCrE}	electrostatic work required to transfer an ion across the electrode/electrolyte interface (part of the Galvani potential)
E_T	the difference between the measured cell potential (E) and surface potential (ψ_0)
ΔG	the free energy difference for the cell
ΔG°	The free energy difference of the cell in the equilibrium state ($\Delta G = 0$)
Q	Reaction coefficient (equivalent of the equilibrium constant for non-equilibrium condition)
K_+, K_1, K_2	Surface protonation equilibrium constant
α, β	Parameter describing deviation for the slope of the surface potential from Nernstian model
E^{ab}	the measured cell potential in alkalimetric titration (ab: from acidic pH to basic pH)
E^{ba}	the measured cell potential in acidimetric titration (ba: from basic pH to acidic pH)
ΔG^{ab}	the free energy of the cell in alkalimetric titration
ΔG^{ba}	The free energy surface in acidimetric titration
ψ_0^{ab}	Surface potential obtained in the alkalimetric titration
ψ_0^{ba}	Surface potential obtained in the acidimetric titration
$I(\zeta)$	The area difference between left and right-hand sided of titration loop with respect to the position of dividing surface (ζ)
α_i	Surface potential nonlinearity coefficients in perturbative expansion
ζ	Integration variable (pH) in the titration hysteresis analysis method
IEP	Isoelectric point, defined as the value of pH at which electrokinetic potential (ζ) is equal 0, pHIEP
PZP	Point of zero potential, defined as the pH value at which ($\psi_0 = 0$), pH _{PZP}
PZC	Point of zero charge, defined as the pH value at which ($\sigma_0 = 0$), pH _{PZC} (extended classification can be found in Reference 32)
PZSE	Point of Zero Salt Effect, pH at which potentiometric titration curves obtained for various electrolyte concentration intersect, pH _{PZSE}

REFERENCES

- W. Stumm and J. J. Morgan, *Aquatic Chemistry*, Wiley, New York, 1996.
- D. A. Dzombak and F. M. M. Morel, *Surface Complexation Modeling: Hydrous Ferric Oxide*, Wiley, 1990.
- P. Zarzycki, *J. Phys. Chem. C* **111** (2007) 7692–7703.
- P. W. Schindler, B. Fürst, R. Dick, and P. U. Wolf, *J. Colloid Interface Sci.* **55** (1976) 469–475.
- S. Žalac and N. Kallay, *J. Colloid Interface Sci.* **149** (1992) 233–240.
- T. Preočanin and N. Kallay, *Croat. Chem. Acta* **71** (1998) 649.
- A. V. Delgado, *Interfacial Electrokinetics and Electrophoresis*, M. Dekker, Basel, 2002.
- M. Ciobanu, J. P. Wilburn, M. L. Krim, and D. E. Clifflin in: C. G. Zoski (Ed.) *Handbook of Electrochemistry*, Elsevier, 2007.
- C. M. A. Brett and A. M. O. Brett, *Electrochemistry: Principles, Methods, and Applications*, Oxford University Press, Oxford, 1993.
- L. Bousse, N. F. de Rooij, and P. Bergveld, *IEEE Trans. Electron Devices* **30** (1983) 1263–1270.
- L. Bousse, N. F. de Rooij, and P. Bergveld, *Surf. Science* **135** (1983) 479–496.
- R. E. G. van Hal, J. C. T. Eijkel, and P. Bergveld, *Adv. Colloid Interface Sci.* **69** (1996) 31–32.
- N. H. G. Panners, L.K. Koopal, and J. Lyklema, *Colloids and Surfaces* **21** (1986) 457–468.
- M. J. Avena, O. R. Camara, and C. P. de Pauli, *Colloids and Surfaces* **69** (1993) 217–228.
- E. Kinoshita, F. Ingman, and G. Edwall, *Electrochim. Acta* **31** (1986) 29–38.
- W. T. Grubb and L. H. King, *Anal. Chem.* **52** (1980) 270–273.
- N. Kallay, Z. Dojnovič, and A. Čop, *J. Colloid Interface Sci.* **286** (2005) 610–614.
- T. Preočanin, A. Čop, and N. Kallay, *J. Colloid Interface Sci.* **299** (2006) 772–776.
- N. Kallay and T. Preočanin, *J. Colloid Interface Sci.* **318** (2008) 290–295.
- N. Kallay, T. Preočanin, and T. Ivšić, *J. Colloid Interface Sci.* **309** (2007) 21–27.
- N. Kallay, T. Preočanin, A. Selmani, F. Šupljika, and I. Leniček *Croat. Chem. Acta* **82** (2009) 323–327
- N. Kallay and S. Žalac, *J. Colloid Interface Sci.* **230** (2000) 1–11.
- R. K. Quinn, R.D. Nasby, and R.J. Baughman, *Mater. Res. Bull.* **11** (1976) 1011–1017.

24. N. Kallay and D. Čakara, *J. Colloid Interface Sci.* **232** (2000) 81–85.
25. N. Kallay, A. Čop, E. Chibowski, and L. Holysz, *J. Colloid Interface Sci.* **259** (2003) 89–96.
26. N. Kallay, T. Preočanin, and F. Šupljika, *J. Colloid Interface Sci.* **327** (2008) 384–387.
27. T. Preočanin, F. Šupljika, and N. Kallay, *J. Colloid Interface Sci.* **346** (2010) 222–225.
28. S. Trasatti (Ed.), *Pure Appl. Chem.* **58** (1986) 956–966.
29. H.-H. Butt, K. Graf, and M. Kappl, *Physics and Chemistry of Interfaces*, Wiley, New York, 2003, chapter 5, pp 63–65.
30. P. Zarzycki and K. M. Rosso, *J. Colloid Interface Sci.* **341** (2010) 143–152.
31. P. Zarzycki, R. Charnas, and P. Szabelski, *J. Comput. Chem.* **25** (2004) 704–711.
32. G. Sposito, *Environ. Sci. Technol.* **32** (1998) 2815–2819.
33. W. H. van Riemsdijk, J. C. M. de Wit, L. K. Koopal, and G. H. Bolt, *J. Colloid Interface Sci.* **116** (1987) 511–522.
34. P. Zarzycki, *Appl. Surface Sci.* **253** (2007) 7604–7612.
35. D. E. Yates and S. L. T. W. Healy, *J. Chem. Soc., Faraday Trans. 1* **70** (1974) 1807–1818.
36. D. Chan, J. W. Perram, L. R. White, and T. W. Healy, *J. Chem. Soc., Faraday Trans. 1* **71** (1975) 1046–1057.
37. T. Hiemstra, W. H. Van Riemsdijk, and G.H. Bolt, *J. Colloid Interface Sci.* **133**(1989) 91–104.
38. T. Hiemstra, J. C. M. de Wit, and W. H. van Riemsdijk, *J. Colloid Interface Sci.* **133** (1989) 105–117.
39. D. P. Landau and K. Binder, *A guide to Monte Carlo simulations in statistical physics*, 2nd edition, Cambridge University Press, Cambridge, 2000.
40. D. Nicholson and N. G. Personage, *Computer Simulation and the Statistical Mechanics of Adsorption*, Academic Press, London 1982.
41. D. W. Heermann, *Computer Simulation Methods in Theoretical Physics*, Springer, Berlin, 1990.
42. M. Borkovec, *Langmuir* **13** (1997) 2608–2613.
43. M. Borkovec, J. Daicic, G. J. M. Koper, *Physica A* **298** (2001) 1–23.
44. P. Zarzycki, P. Szabelski, and R. Charnas, *J. Comput. Chem.* **26** (2005) 1079–1088.
45. P. Zarzycki, *J. Colloid Interface Sci.* **306** (2007) 328–336.
46. P. Zarzycki, P. Szabelski, and R. Charnas, *Appl. Surface Sci.* **252** (2005) 752–758.
47. P. Zarzycki, *J. Colloid Interface Sci.* **315** (2007) 54–62.
48. P. Zarzycki and K.M. Rosso, *Langmuir* **25** (2009) 6841–6848.
49. P. Zarzycki, *J. Colloid Interface Sci.* **311** (2007) 622–627.
50. P. Zarzycki, *Langmuir* **22** (2006) 11234–11240.
51. J. R. Rustad, A. R. Felmy, and B. P. Hay, *Geochim. Cosmochim. Acta* **60** (1996) 1553–1562.
52. J. R. Rustad, A. R. Felmy, and E. J. Bylaska, *Geochim. Cosmochim. Acta* **67** (2003) 1001–1016.
53. M. Předota, P. T. Cummings, and D. J. Wesolowski, *J. Phys. Chem. C* **111**, (2007) 3071–3079.
54. M. Předota, Z. Zhang, P. Fenter, D.J. Wesolowski, and P.T. Cummings, *J. Phys. Chem. B* **108** (2004) 12061–12072.
55. M. Předota, A. V. Bandura, P. T. Cummings, J. D. Kubicki, D. J. Wesolowski, A. Chialvo, and M. L. Machesky, *J. Phys. Chem. B* **108** (2004) 12049–12060.
56. P. Zarzycki, S. Kerisit, and K. M. Rosso, *J. Phys. Chem. C* **114** (2010) 8905–8916.
57. P. Zarzycki and K. M. Rosso, *J. Phys. Chem. C* **114** (2010) 10019–10026.
58. E. Spohr, *Electrochim. Acta* **49** (2003), 23–27.
59. A. A. Kornyshev, E. Spohr, and M. A. Vorotyntsev, *Electrochemical Interfaces: At the Border Lin*, in: A. J. Bard, M. Stratmann, E. Gileadi and M. Urbakh (Eds), *Encyclopedia of Electrochemistry*, Wiley-VCH: New York, 2002; pp. 33–132.
60. E. Spohr, *Computer simulation of the structure and dynamics of water near metal surfaces*, in: G. Jerkiewicz, M. P. Soriaga, K. Uosaki, and A. Wieckowski (Eds), *Solid-Liquid Electrochemical Interfaces*, ACS Symposium Series 656; American Chemical Society; Washington, DC, 1996; pp. 31–44.
61. M. L. Berkowitz, I.-C. Yeh, and E. Spohr, *Structure of water at the water-metal interface: molecular dynamics computer simulations*, in: A. Wieckowski (Ed.), *Interfacial Electrochemistry: Theory, experiment, and applications*, Dekker: New York, 1999, pp. 33–45.
62. E. Spohr, *Electrochim. Acta* **44** (1999) 1697–1705.
63. M. R. Philpott and J. N. Glosi, *Molecular Dynamics Simulation of Interfacial Electrochemical Processes: Electrical Double Layer Screening*, in: G. Jerkiewicz, M. P. Soriaga, K. Uosaki, and A. Wieckowski (Eds), *Solid-Liquid Electrochemical Interfaces*, ACS Symposium Series 656; American Chemical Society; Washington, DC, 1996; pp. 12–30.
64. J. N. Glosi and M. R. Philpott, *Electrochim. Acta* **41** (1996) 2145–2158.
65. M. R. Philpott and J. N. Glosi, *J. Electroanal. Chem.* **409** (1996) 65–72.
66. N. Kallay, T. Preočanin, D. Kovačević, J. Lützenkirchen, and E. Chibowski, *Croat. Chem. Acta* (2010) in press.
67. W. Janusz, *Electrical Double-Layer at Oxide-Solution Interfaces*, in: A. T. Hubbard (Ed.), *Encyclopedia of Surface and Colloid Science*, volume II, Marcel Dekker, New York, 2000.
68. M.-C. Jodin, F. Gaboriaud, and B. J. Humbert, *Colloid Interface Sci.* **287** (2005) 581–591.
69. S. R. Mehr, D. J. Eatough, L. D. Hansen, and E. A. Lewis, *Thermochimica Acta* **154** (1989) 129–143.
70. P. Zarzycki, T. Preočanin, K. M. Rosso, and S. Chatman, *Science* (2010) submitted.
71. G. Bertotti, *Hysteresis in Magnetism*, Academic Press, San Diego, 1998.
72. B. Prelot, R. Charnas, P. Zarzycki, F. Thomas, F. Villieras, W. Piasecki, and W. Rudzinski, *J. Phys. Chem. B* **106** (2002) 13280–13286.
73. R. Charnas, P. Zarzycki, F. Villieras, F. Thomas, B. Prelot, and W. Piasecki, *Colloids Surf. A* **244** (2004) 9–17.
74. S. V. Yanina and K. M. Rosso, *Science* **320** (2008) 218–222.
75. M. A. Blesa, P. J. Morando, and A. E. Regazzoni, *Chemical Dissolution of Metal Oxides*, CRC, Boca Raton, 1994.
76. P. Zarzycki, R. Charnas, and W. Piasecki, *Adsorption* **10** (2004) 139–149.
77. W. Janusz, I. Kobal, A. Sworska, and J. Szczypa, *J. Colloid Interface Sci.* **187** (1997) 381–387.
78. A. Breeuwsma and J. Lyklema, *Discuss. Faraday Soc.* **52** (1971) 324–333
79. S. Mustafa, B. Dilera, Z. Neelofer, A. Naeem, and S. Tasleem, *J. Colloid Interface Sci.* **204** (1998) 284–293.
80. N. Kallay, T. Preočanin, and T. Ivšić, *J. Colloid Interface Sci.* **309** (2007) 21–27.
81. V. May and O. Kuhn, *Charge and Energy Transfer Dynamics in Molecular Systems*, 2nd edition, Wiley, New York, 2004.
82. A. Nitzan, *Chemical Dynamics in Condensed Physics*, Oxford University Press, Oxford, 2006.
83. P. Zarzycki, W. Piasecki, and K.M. Rosso, in preparation.
84. K. M. Rosso, S. V. Yanina, C. A. Gorski, P. Larese-Casanova, and M. M. Scherer, *Environ. Sci. Technol.* **44** (2010) 61–67.
85. G. King and A. Warshel, *J. Chem. Phys.* **93** (1990) 8682–8692.
86. P. Zarzycki, S. Kerisit, and K. M. Rosso, in preparation.

SAŽETAK**Teorija, eksperiment i kompjuterska simulacija elektrostatskog potencijala na međupovršini kristal/elektrolit**

**Piotr Zarzycki,^a Kevin M. Rosso,^a Shawn Chatman,^a
Tajana Preočanin,^b Nikola Kallay^b i Wojciech Piasecki^c**

^a*Chemical and Materials Sciences Division, Pacific Northwest National Laboratory,
Richland, WA 99354, USA*

^b*Zavod za fizikalnu kemiju, Kemijski odsjek, Prirodoslovno-matematički fakultet,
Sveučilište u Zagrebu, HR 10000 Zagreb, Hrvatska*

^c*Department of Biochemistry, The Jozef Pilsudski Academy of Physical Education, Warsaw, Poland*

U ovom članku razmatrani su napredak i izazovi kod mjerenja, analiziranja i tumačenja nastanka elektrostatskog potencijala na međupovršini kristal/elektrolit. Analizirani su različiti modeli površinskog kompleksiranja, prikazana je metoda za procjenu točke nul-potencijala za plohu monokristala uz pomoć histereze do koje dolazi tijekom pH titracije, te porijeklo nelinearne ovisnosti površinskog potencijala o pH. Poznato je da elektrostatski potencijal znatno ovisi o mnogim pojavama poput heterogenosti površine, transformacijama na površini, reakcijama prijenosa naboja i dodatnog skoka potencijala na rubovima kristalne plohe i/ili Schottkyjevim barijerama. Potencijal monokristalnelektrode je također osjetljiv na te pojave što otežava tumačenje rezultata mjerenja. Predloženi analitički model titracijske histereze i novi Model površinskog kompleksiranja koji uzima u obzir procese prijenosa naboja doprinose tumačenju eksperimentalnih podataka i osiguravaju jednoznačno tumačenje elektrostatskog odziva nepolarizabilnih monokristalnih elektroda.